

## Experimental and theoretical studies of isolated neutral and ionic 2-propanol and their clusters

Joong-Won Shin and Elliot R. Bernstein

Citation: *The Journal of Chemical Physics* **130**, 214306 (2009); doi: 10.1063/1.3148378

View online: <http://dx.doi.org/10.1063/1.3148378>

View Table of Contents: <http://aip.scitation.org/toc/jcp/130/21>

Published by the *American Institute of Physics*

---

---

**COMPLETELY**

**REDESIGNED!**



**PHYSICS  
TODAY**

*Physics Today* Buyer's Guide  
Search with a purpose.

## Experimental and theoretical studies of isolated neutral and ionic 2-propanol and their clusters

Joong-Won Shin and Elliot R. Bernstein<sup>a)</sup>

Department of Chemistry, Colorado State University, Fort Collins, Colorado 80523-1872, USA

(Received 9 March 2009; accepted 12 May 2009; published online 5 June 2009)

Infrared plus vacuum ultraviolet (IR/VUV) nonresonant photoionization spectroscopy and VUV/IR photodissociation spectroscopy are employed to study fragmentation pathways and structures of neutral and ionic 2-propanol ((CH<sub>3</sub>)<sub>2</sub>CHOH) (IPA) and their relevant clusters of size up to the pentamer. Only the *gauche* monomer is generated in the supersonic expansion; its VUV induced fragmentation pathways involve C<sub>α</sub>-C<sub>β</sub> bond dissociation. The clusters consist of both *gauche* and *trans* conformers and their VUV induced fragmentation pathways are size dependent. The IR spectra of neutral clusters (IPA)<sub>n</sub> suggest that the dimer has a chainlike structure, whereas larger clusters have cyclic structures. VUV ionization of the neutral *gauche* 2-propanol generates two parent cation isomers whose C<sub>α</sub>-C<sub>β</sub> bond dissociations are facilitated by excitation of the OH vibrations. The IR spectra of ionic molecular complex clusters (IPA)<sub>n-1</sub>·CH<sub>3</sub>CHOH<sup>+</sup> and protonated clusters (IPA)<sub>n-1</sub>·H<sup>+</sup>, generated by VUV ionization of neutral clusters, show that both cluster types adopt open structures with at least one free OH group. Qualitative structural assignments are generated for the neutral species based on MP2/aug-cc-pVDZ, MP2/6-31G, and B3LYP/6-31+G(d) calculations. © 2009 American Institute of Physics. [DOI: 10.1063/1.3148378]

### I. INTRODUCTION

Hydrogen bonding structures in gas phase clusters are prototypical models for understanding molecular interactions in condensed phase media. Water clusters (H<sub>2</sub>O)<sub>n</sub> and methanol clusters (CH<sub>3</sub>OH)<sub>n</sub> have been subjects of considerable attention in this respect, and their structures have been extensively investigated by various experimental<sup>1-23</sup> and theoretical<sup>24-32</sup> approaches. A general morphological trend in these clusters is that they undergo structural changes from chainlike to closed or cyclic structures as the cluster size increases; this rearrangement maximizes the number of hydrogen bonds. The extent of hydrogen bonding can be directly investigated by employing infrared (IR) spectroscopy to detect the OH stretching modes of the relevant clusters. The OH vibration is very susceptible to local perturbations and will show a dramatic energy redshift when the OH group in question is strongly hydrogen bonded to an accepting group, such as an OH group of an adjacent water or alcohol molecule.<sup>7,9,22,33</sup> The individual redshifted OH stretches of sufficiently large clusters<sup>22,33-36</sup> eventually merge into one broad profile similar to that observed for a condensed phase. This broad profile is known as an “icelike” feature<sup>34</sup> and represents condensed phase behavior of the clusters. Free OH stretching features in the cluster spectra are indicative of gas phase behavior. Therefore, clusters essentially serve as an important bridge system between condensed and gas phase media.

Protonated hydrogen bonded clusters (ROH)<sub>n-1</sub>·H<sup>+</sup>,  $n \geq 2$  (R=H, CH<sub>3</sub>, CH<sub>2</sub>CH<sub>3</sub>, etc.) are another species of great interest;<sup>12,21,22,32,36-43</sup> their structures can accommodate ei-

ther the Eigen<sup>44</sup> or Zundel<sup>45</sup> type ion. Similar to their neutral analogs, the IR spectra of these ions in the OH stretch region show that large clusters have closed structures dominated by complex hydrogen bonding interactions, whereas smaller clusters adopt chainlike structures.<sup>22,33,37-42</sup> Transformation from chainlike to closed structures for protonated clusters occurs, however, at sizes different from those for neutral species due to the presence of an extra positive charge.<sup>22,33,42</sup> While there are different techniques available for generating protonated clusters, a previous study<sup>20</sup> has shown that VUV ionization of (ROH)<sub>n</sub> clusters leads to the formation (ROH)<sub>n-1</sub>·H<sup>+</sup> clusters with mass spectral intensities that reflect the neutral parent cluster population distribution. VUV soft ionization also produces ionic molecular complex clusters for alcohols larger than methanol.<sup>43</sup>

In the present study, we perform infrared plus vacuum ultraviolet (IR/VUV) nonresonant photoionization spectroscopy for neutral 2-propanol and its clusters (IPA)<sub>n</sub> in the size range  $n=1-5$  and VUV/IR photodissociation spectroscopy of ionic 2-propanol (IPA) and its cluster related species [ionic molecular complex clusters (IPA)<sub>n-1</sub>·CH<sub>3</sub>CHOH<sup>+</sup> and protonated clusters (IPA)<sub>n-1</sub>·H<sup>+</sup>]. IPA provides additional complexity to our previously investigated methanol<sup>21,22</sup> and ethanol<sup>33</sup> cluster series due to the presence of an extra methyl group, the existence of two conformers (*gauche* and *trans*), and various possible isomers that can arise therefrom. Fragmentation pathways of the IPA related species are deduced from time of flight (TOF) mass spectra, and isomer assignments are made based on the analysis of IR spectra for the CH and OH stretching regions. The experimental data are complemented with *ab initio* and density functional theory (DFT) calculations.

<sup>a)</sup>Author to whom correspondence should be addressed. Electronic mail: erb@lamar.colostate.edu.

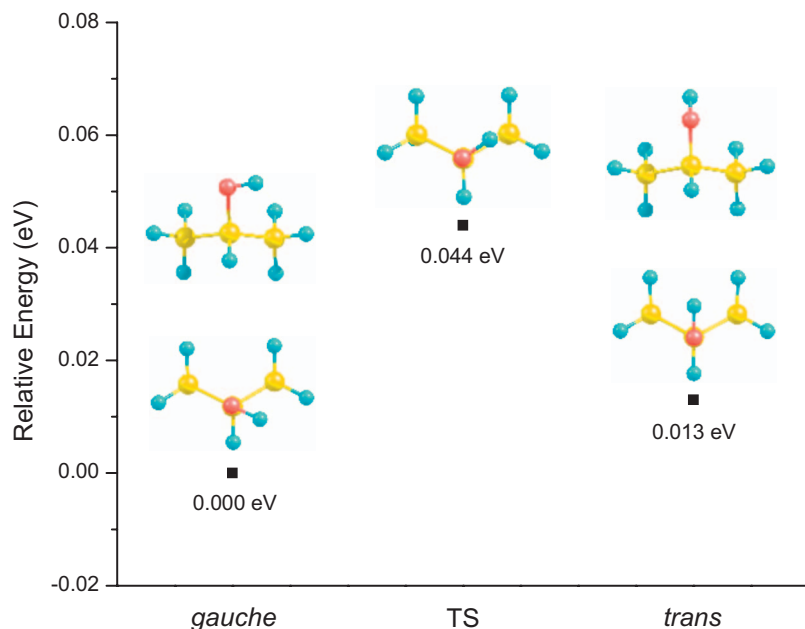


FIG. 1. (Color) MP2/aug-cc-pVDZ structures (two views) of *gauche*-, *trans*-IPA molecules, and the transition state between the two. The energy values are zero point corrected. The lower structures for the *gauche* and *trans* conformers are viewed along the O–C<sub>α</sub> bond.

## II. EXPERIMENTAL PROCEDURES

The experimental apparatus has been described previously in detail.<sup>21,22,33</sup> The IPA monomer and its hydrogen bonded clusters are prepared by supersonic expansion of IPA seeded in a Kr/He mixture (15%/85%, 40 psi backing pressure) using a Jordan Co. valve. The molecular beam is collimated by a 1.5 mm aperture diameter skimmer and is crossed by IR and VUV beams in the photointeraction region of the TOF mass spectrometer (TOFMS). The vertical ionization energy (VIE) of an IPA molecule is 10.44 eV,<sup>46</sup> which is slightly less than the ionizing VUV photon energy employed in this study.

The VUV radiation [118 nm, ninth harmonic of Nd:YAG (yttrium aluminum garnet) fundamental, 10.49 eV,  $\sim 1 \mu\text{J}/\text{pulse}$ , with the conversion efficiency of  $\sim 1.2 \times 10^{-5}$  (Ref. 20)] is generated by exciting Xe in a Xe/Ar mixture (1:10,  $\sim 200$  Torr) with the third harmonic (355 nm,  $\sim 30$  mJ/pulse) of the fundamental beam. Tunable IR radiation (3–5 mJ/pulse in the 2800–3800  $\text{cm}^{-1}$  range with a bandwidth of  $\sim 2$   $\text{cm}^{-1}$ ) is generated from an optical parametric oscillator/optical parametric amplifier (OPO/OPA) system (LaserVision) pumped by the Nd:YAG fundamental and counterpropagates with respect to the VUV beam. Both the VUV and IR laser beams are perpendicular to the molecular beam and to the ion flight path of the TOFMS.

In order to obtain IR spectra of neutral species, the IR beam is timed to precede the VUV beam by approximately 70 ns. Neutral molecule and cluster fragmentations can be observed as changes in mass spectral intensities of the VUV ionization products when the IR energy is in resonance with their vibrational modes. In particular, vibrational excitation of a neutral molecule changes its VUV induced fragmentation efficiencies, and vibrational excitation of a neutral cluster decreases its population through photofragmentation into smaller sized cluster mass channels, which results in increased populations for the latter. This also influences the IR spectra. Such fragmentation from a larger to a smaller cluster upon IR absorption would be detected as a positive rather

than negative contribution to the detected IR spectrum in the lower mass channel. The IR beam is delayed by approximately 20 ns with respect to the VUV beam to acquire IR spectra of ionic species. Similar to the case of neutral species, fragmentation from a larger to a smaller ionic cluster due to IR absorption would be detected as a positive contribution to the IR spectrum of the smaller cluster.

Each spectrum is an accumulation of multiple scans. The IR beam path is purged with N<sub>2</sub> gas to minimize ambient atmospheric IR absorption.

## III. COMPUTATIONAL METHODS

All calculations are performed using the GAUSSIAN 03 (Ref. 47) program on Colorado State University's Chem-Cluster and on the TeraGrid<sup>48</sup> supercomputer system. Geometry optimizations and harmonic vibrational energy calculations of the neutral and ionic IPA monomers are carried out at the MP2/aug-cc-pVDZ level, and transition states are calculated using the QST3 method. Geometry optimizations and harmonic vibrational energy calculations for neutral dimer isomers are also carried out at the same level of theory and basis set. The reported MP2/aug-cc-pVDZ energies are zero point corrected and the vibrational energies are scaled by 0.9593, which is the ratio of experimental<sup>49</sup> and theoretical methanol free OH stretches.

Geometry optimizations of the neutral IPA monomer, dimer, trimer, and tetramer structures for relative energy comparison are carried out at the B3LYP/6-31+G(d) level. Tetramer structures are initially obtained from MP2/6-31G calculations, and the lowest energy structure in each isomer type is reoptimized at the B3LYP/6-31+G(d) level. Basis set superposition errors are corrected by counterpoise calculations, and no zero point corrections are applied.

## IV. RESULTS AND DISCUSSION

IPA has two stable conformers: *gauche* and *trans* (Fig. 1). The difference between the two is that in the *gauche*

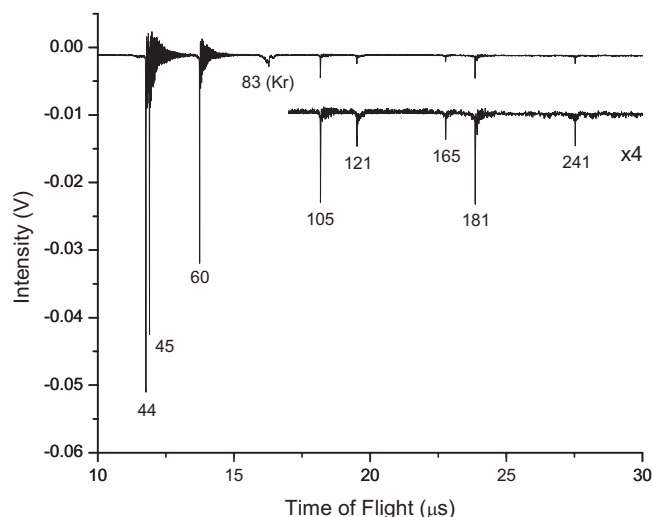
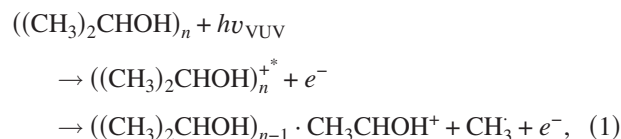


FIG. 2. TOF mass spectrum showing VUV ionization products of the IPA monomer and clusters. The  $m/z=83$  amu ion is the ionized Kr atom in the carrier gas mixture.

conformation, the dihedral angle between the OH hydrogen and  $C_\alpha$ H hydrogen is  $64^\circ$ , whereas this angle is  $180^\circ$  in the *trans* conformation. These conformers are very close in energy; the calculated potential barrier between the two is 0.044 eV. A vibrational spectroscopic study of IPA in a gas cell<sup>50</sup> has shown that both isomers coexist in the gas phase; in a supersonic expansion,<sup>35</sup> all IPA molecules are quenched to the global minimum *gauche* conformer. As will be shown through the analysis of the IR spectra, only the *gauche* IPA conformer is observed in the current study. Figure 2 shows a TOF mass spectrum of the VUV ionized IPA monomer and its clusters. The mass of a single IPA molecule is 60 amu, so the ions at the  $m/z=44$ , 45, and 60 amu mass channels are VUV ionization products derived from (perhaps not exclusively) the IPA monomer. The  $m/z=44$  and 45 amu ions are from the losses of  $CH_4$  (16 amu) and  $CH_3$  (15 amu), respectively, from the monomer as a result of  $C_\alpha-C_\beta$  bond dissociation. The  $m/z=60$  amu ion is the parent IPA cation. The

loss of  $CH_4$  involves hydrogen transfer from the  $C_\alpha$ H group to the dissociating  $CH_3$  group. The 0.05 eV excess energy in the system after VUV ionization is removed from the system in the form of photoelectron kinetic energy, and the excess vibrational energy [vertical ionization energy minus adiabatic ionization energy (VIE–AIE)] leads to the hydrogen transfer and/or  $C_\alpha-C_\beta$  bond dissociation as the Franck–Condon cation evolves to the adiabatic state. Theoretical investigations (Fig. 3) of the two fragmentation channels indicate that the loss of  $CH_3$  is, in fact, a barrierless reaction, while the hydrogen transfer involved in the loss of  $CH_4$  has a barrier of 0.031 eV. This small barrier can be easily overcome during the rearrangement of the Franck–Condon cation to the adiabatic cation following VUV ionization. In both instances, the relatively large energy difference between the Franck–Condon and adiabatic cations can drive the  $C_\alpha-C_\beta$  bond dissociation.

Cations that are associated with IPA clusters are also observed in the mass spectrum (Fig. 2). There are two series of VUV ionization products of the clusters in the mass spectrum:  $((CH_3)_2CHOH)_{n-1} \cdot CH_3CHOH^+$ ,  $n=2$  and 3 (ions at  $m/z=105$  and 165 amu), and  $((CH_3)_2CHOH)_{n-1} \cdot H^+$ ,  $n=3-5$  (ions at  $m/z=121$ , 181, and 241 amu). The ionic molecular complex clusters  $((CH_3)_2CHOH)_{n-1} \cdot CH_3CHOH^+$  are the  $C_\alpha-C_\beta$  bond dissociation products generated according to the reaction



in which  $(CH_3)_2CHOH)_n^+$  are the Franck–Condon cations with excess vibrational energy above the adiabatic ion ground state (on the  $D_0$  potential energy surface). The protonated IPA clusters  $((CH_3)_2CHOH)_{n-1} \cdot H^+$  originate from the  $((CH_3)_2CHOH)_n$  clusters according to the reaction

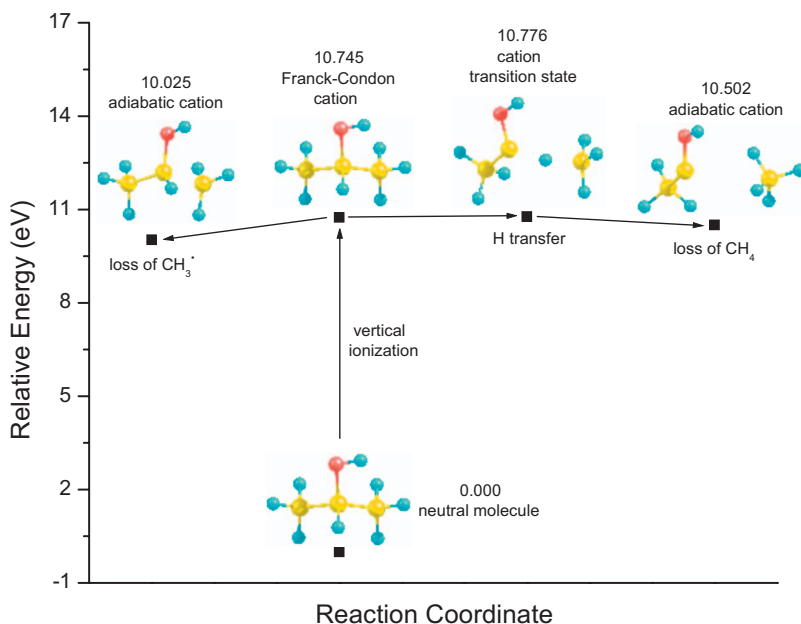


FIG. 3. (Color) MP2/aug-cc-pVDZ calculations for *gauche*-IPA cation fragmentation pathways. Energetics involving the loss of  $CH_4$  and  $CH_3$  for generation of ions observed at  $m/z=44$  and 45 amu, respectively, in the TOF mass spectrum are plotted for their respective reaction coordinates.

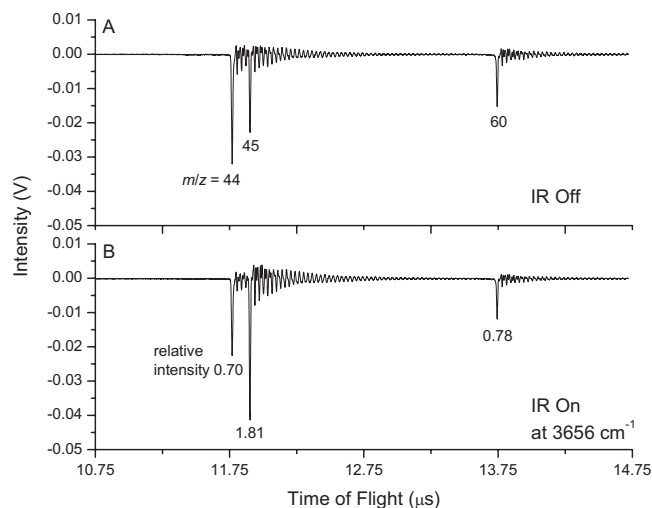
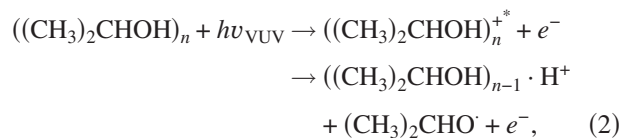


FIG. 4. TOF mass spectrum showing intensity changes in IPA monomer fragment and parent ions (a) without and (b) with the IR energy at  $3656\text{ cm}^{-1}$ , which is the OH stretch energy of a *gauche*-IPA monomer. The relative intensities indicated in the lower spectrum are ratios of the ion intensities with the IR on to those with the IR off.



in which proton transfer and bond dissociation occur as the Franck–Condon cation evolves to the adiabatic state. Reaction (1) is observed for  $n=2$  and 3 clusters, and reaction (2) is observed for  $n=3$ –5 clusters. While the cations generated in the two above reactions may also be fragmentation products of  $((\text{CH}_3)_2\text{CHOH})_{n+1}$ , etc., clusters, our previous study<sup>21</sup> of methanol clusters shows that the population of clusters that undergo more than one monomer evaporation following VUV ionization is insignificant [less than 8% for  $(\text{CH}_3\text{OH})_n$  clusters in the size range of  $3 \leq n \leq 8$ ]. Both reactions occur for the trimer, as indicated by the presence of ions at the  $m/z=121$  and 165 amu mass channels. Their similar mass spectral intensities (1:0.93) imply that either the potential barrier heights associated with these reactions in the trimer are similar or that different cluster isomer types are generated in the molecular beam, with each type fragmenting into a different ion channel. As will be shown later, the latter possibility is in agreement with the trimer IR spectra. Only the protonated species are observed for larger clusters ( $m/z=181$  and 241 amu) because either the potential barrier in reaction (1) increases or the proton affinity of the  $(\text{IPA})_{n-1}$  core increases with the increasing cluster size  $n$ . A similar trend is observed in previous studies of ethanol,<sup>33</sup> 1-propanol,<sup>43</sup> butanol isomers,<sup>51</sup> acetic acid,<sup>52</sup> and propanoic acid,<sup>53</sup> in which small sized clusters primarily undergo the  $\text{C}_\alpha$ – $\text{C}_\beta$  bond dissociation, while larger ones favor the proton transfer/fragmentation reaction (2).

### A. IR/VUV photoionization spectroscopy of neutral IPA monomer and clusters

Figure 4 shows the mass spectra of VUV ionized IPA monomer products, with and without the presence of IR pho-

tons. Absorption of an IR photon by an IPA molecule at the free OH vibrational energy level ( $3656\text{ cm}^{-1}$ ) results in a decrease in the intensities of the  $m/z=44$  and 60 amu ion signals and an increase in the  $m/z=45$  amu ion signal. Since IPA molecules in clusters are expected to be bound together by hydrogen bonding, their OH stretches are redshifted below  $3656\text{ cm}^{-1}$  and so the mass spectral intensity changes observed in Fig. 4 are not associated with absorption of IR photons by clusters. The monomer acquires an internal energy of 0.45 eV ( $3656\text{ cm}^{-1}$ ) as a result of the OH stretch excitation, and this extra energy facilitates the  $\text{C}_\alpha$ – $\text{C}_\beta$  bond dissociation when a VUV photon ionizes the monomer. Thus, the parent ion at  $m/z=60$  amu loses intensity, while the  $m/z=45$  amu ion gains intensity. On the other hand, the  $m/z=44$  amu ion intensity decreases under this condition most likely because the extra vibrational energy in the molecule enhances the direct  $\text{C}_\alpha$ – $\text{C}_\beta$  bond breaking reaction at the expense of the parent ion and the hydrogen transfer/loss of  $\text{CH}_4$  reaction channel. Note that changes in the mass spectral intensities of the  $m/z=44$ , 45, and 60 amu ions should be conserved within the experimental uncertainty. A summation of decreases observed for the  $m/z=44$  and 60 amu ion intensities and the original  $m/z=45$  amu ion intensity (i.e., its ion intensity without the presence of IR photons) is within  $\sim 10\%$  of the  $m/z=45$  amu ion intensity in the presence of  $3656\text{ cm}^{-1}$  IR photons.

IR spectra of the IPA monomer, which are acquired by monitoring the monomer ion mass channels  $m/z=44$ , 45, and 60 amu while scanning the IR laser in the  $2800$ – $3800\text{ cm}^{-1}$  region, are presented in Figs. 5(a)–5(c), and the scaled harmonic frequencies of *gauche* and *trans* conformers are shown in Figs. 5(d) and 5(e). The experimental and theoretical vibrational energy values are listed in Table I. In Figs. 5(a)–5(c), the sharp intense peaks at  $3656\text{ cm}^{-1}$  correspond to the free OH stretch, and broad transitions in the  $3200$ – $3440\text{ cm}^{-1}$  region are OH stretching modes of clusters fragmenting into these mass channels. The IR radiation in the latter region excites hydrogen bonded OH stretches of the clusters that result in the loss of one (or more) IPA molecule(s) via intermolecular vibrational redistribution (IVR) and cluster vibrational predissociation. The CH stretch region is congested due to contributions from both monomer and clusters, as evidenced by the presence of both dips and enhancements in the  $2860$ – $3000\text{ cm}^{-1}$  region. Similar to the observations involving the free OH stretch at  $3656\text{ cm}^{-1}$ , the dips in the CH region detected in the  $m/z=44$  and 60 amu mass channels and the increase in the  $m/z=45$  amu mass channel are related to the populations of the various reaction channels with increased energy in the parent ion. Comparison of our IR spectra and those from previous gas phase studies<sup>35,50</sup> shows that only the *gauche* monomer is generated in the current study. Also, the scaled harmonic OH stretch energy ( $3657\text{ cm}^{-1}$ ) of the *gauche* monomer is in nearly perfect agreement with the value ( $3656\text{ cm}^{-1}$ ) from the IR spectrum, and that ( $3639\text{ cm}^{-1}$ ) of the *trans* monomer is in excellent agreement with the previously reported value ( $3637\text{ cm}^{-1}$ ) (Ref. 50) from a gas cell study as well.

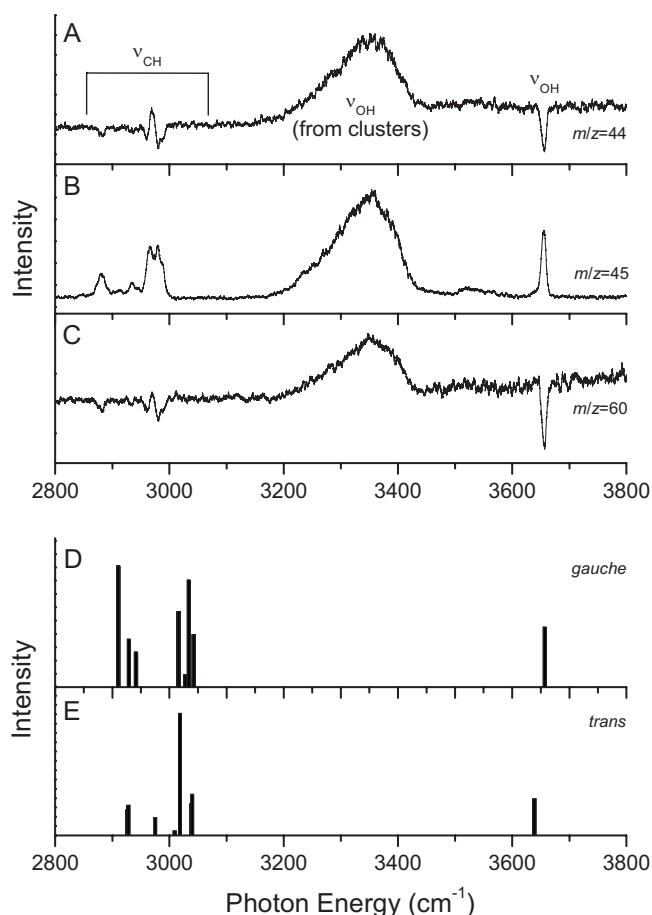


FIG. 5. IR spectra of the neutral IPA monomer obtained by monitoring ion intensity changes of (a)  $m/z=44$  amu, (b)  $m/z=45$  amu, and (c)  $m/z=60$  amu ion mass channels. Free OH stretches of an IPA monomer are observed in all ion channels at  $3656\text{ cm}^{-1}$ , and the broad transitions in the  $3200\text{--}3440\text{ cm}^{-1}$  range are due to IPA monomers fragmented from IPA clusters. The CH stretch region ( $2860\text{--}3000\text{ cm}^{-1}$ ) shows transitions from both monomer and clusters. MP2/aug-cc-pVDZ harmonic vibrational energies of (d) *gauche*- and (e) *trans*-IPA molecules are given. The energies are scaled by 0.9593.

Figure 6 shows IR spectra of IPA clusters  $((\text{CH}_3)_2\text{CHOH})_n$  in the size range of  $n=2\text{--}5$ . The spectra are obtained by monitoring the fragment ion channels  $((\text{CH}_3)_2\text{CHOH})_{n-1}\cdot\text{CH}_3\text{CHOH}^+$  for  $n=2$  and 3 and  $((\text{CH}_3)_2\text{CHOH})_{n-1}\cdot\text{H}^+$  for  $n=3\text{--}5$  while scanning the IR laser in the  $2800\text{--}3800\text{ cm}^{-1}$  range. The broad transitions that appear as dips indicate parent cluster fragmentation; these features gradually redshift with increasing cluster size. The small intensity enhancements just red of the dips indicate that larger clusters are fragmenting into these smaller cluster mass channels. The IR spectrum of the dimer [Fig. 6(a)] shows dips at  $3517$ ,  $3544$  (indicated by the red and green arrows, respectively), and  $3645\text{ cm}^{-1}$ , which correspond to the OH stretches in different environments. The dips result from photofragmentation of the dimer through the loss of one IPA molecule mediated by IVR. These peaks also appear as a weak broad transition near  $3520\text{ cm}^{-1}$  in the monomer IR spectra [Figs. 5(a)–5(c)]. The dimer peak at  $3645\text{ cm}^{-1}$  is redshifted from the free OH stretch of the *gauche* monomer by  $11\text{ cm}^{-1}$ , and this small redshift implies that this transition corresponds to the hydrogen bond accepting free OH

TABLE I. Experimentally obtained free and hydrogen bonded OH stretch ( $\nu_{\text{OH}}$ ) energies of neutral 2-propanol (IPA) monomer and clusters. Harmonic OH stretch energy values of the *gauche*- and *trans*-IPA monomers and of the four dimer isomers are shown for comparison. Calculations are carried out at the MP2/aug-cc-pVDZ level and the vibrational energies are scaled by the factor of 0.9593. *g*=*gauche* and *t*=*trans*. X·Y means X is hydrogen bonded to Y.

Experiment			
$((\text{CH}_3)_2\text{CHOH})_n$	Ion $m/z$	$\nu_{\text{OH}}$ ( $\text{cm}^{-1}$ )	Cluster $\nu_{\text{OH}}$ ( $\text{cm}^{-1}$ ) (center of peak enhancement)
1	44	3656	3351
	45	3655	3354
	60	3656	3348
2	105	3517, 3544, 3645	3414
3	121	3482	3326
	165	3431	3253
4	181	3323	3205
5	241	3292	...
Calculation ( $n=1$ )			
<i>gauche</i> -IPA		3657	...
<i>trans</i> -IPA		3639	...
Calculation ( $n=2$ )			
$(g\text{-IPA})\cdot(g\text{-IPA})$		3483, 3641	...
$(g\text{-IPA})\cdot(t\text{-IPA})$		3502, 3627	...
$(t\text{-IPA})\cdot(g\text{-IPA})$		3462, 3640	...
$(t\text{-IPA})\cdot(t\text{-IPA})$		3480, 3628	...

stretch.<sup>6,24</sup> Since  $3645\text{ cm}^{-1}$  is above the free OH stretch energy of a *trans* monomer, which is at  $3637\text{ cm}^{-1}$  (Ref. 50), the hydrogen bond accepting IPA in the dimer has a *gauche* conformation. The CH vibrations of the dimer are observed near  $2975\text{ cm}^{-1}$  in Fig. 6(a).

The two partially resolved transitions at  $3517$  and  $3544\text{ cm}^{-1}$  are redshifted by  $120$  and  $112\text{ cm}^{-1}$  from the free OH stretches of *trans*- and *gauche*-IPA monomers, respectively ( $3637$  and  $3656\text{ cm}^{-1}$ ); these features must therefore result from the hydrogen bonded (i.e., hydrogen bond donating) OH stretches of both conformers. Assuming that perturbations caused for the OH groups of both monomer types by hydrogen bonding are similar (since they are in similar environments), the  $3517\text{ cm}^{-1}$  feature can be assigned to the OH stretch of hydrogen bond donating *trans*-IPA, and the  $3544\text{ cm}^{-1}$  feature is the OH stretch of hydrogen bond donating *gauche*-IPA. MP2/aug-cc-pVDZ harmonic vibrational energy calculations also support these assignments (Table I). The calculations show that in the case of  $(\textit{gauche}\text{-IPA})\cdot(\textit{gauche}\text{-IPA})$  and  $(\textit{trans}\text{-IPA})\cdot(\textit{gauche}\text{-IPA})$ , the OH vibrational energies of hydrogen bond accepting *gauche*-IPA are at  $3641$  and  $3640\text{ cm}^{-1}$ , respectively, which are in excellent agreement with the experimental value of  $3645\text{ cm}^{-1}$ . The OH vibrational energies of hydrogen bond donating *gauche*- and *trans*-IPA in these clusters are predicted at  $3483$  and  $3462\text{ cm}^{-1}$ , respectively, which are redshifted by  $174$  and  $177\text{ cm}^{-1}$  from their respective calculated free OH stretches. Also note that the peak spacing between the two predicted transitions is  $21\text{ cm}^{-1}$ , which is in very good agreement with

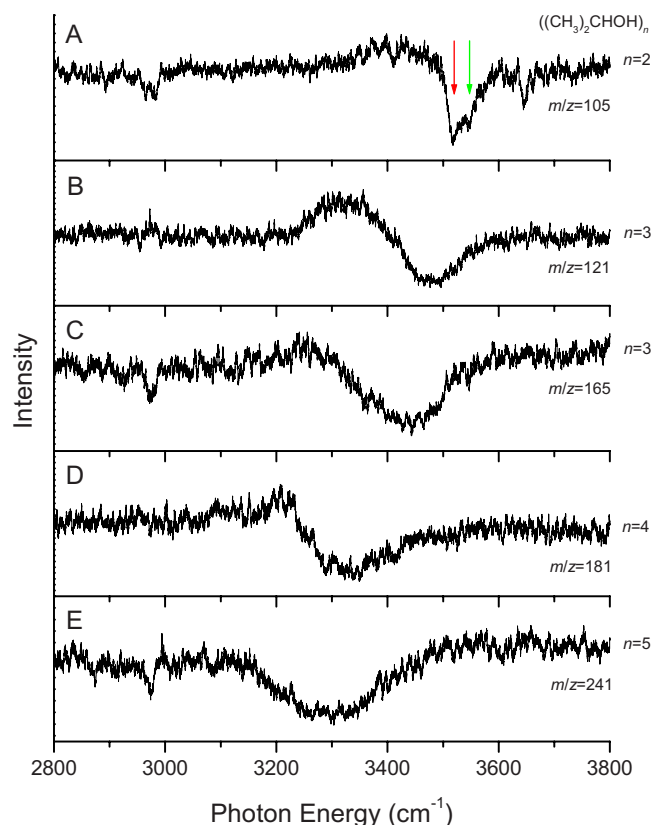


FIG. 6. (Color online) IR spectra of IPA clusters  $((\text{CH}_3)_2\text{CHOH})_n$ ,  $n=2-5$ . In the dimer ( $n=2$ ), one IPA molecule is hydrogen bonded to another: This structure yields a hydrogen bond accepting free OH stretch mode at  $3645\text{ cm}^{-1}$  with hydrogen bonded OH stretch mode features appearing to the red. The red and green arrows in (a) indicate hydrogen bonded OH stretches of *trans*- and *gauche*-IPA monomers, respectively, in dimer clusters. Absence of free OH stretches in the larger clusters ( $n \geq 3$ ) indicates that all their OH groups are involved in the hydrogen bonding interactions.

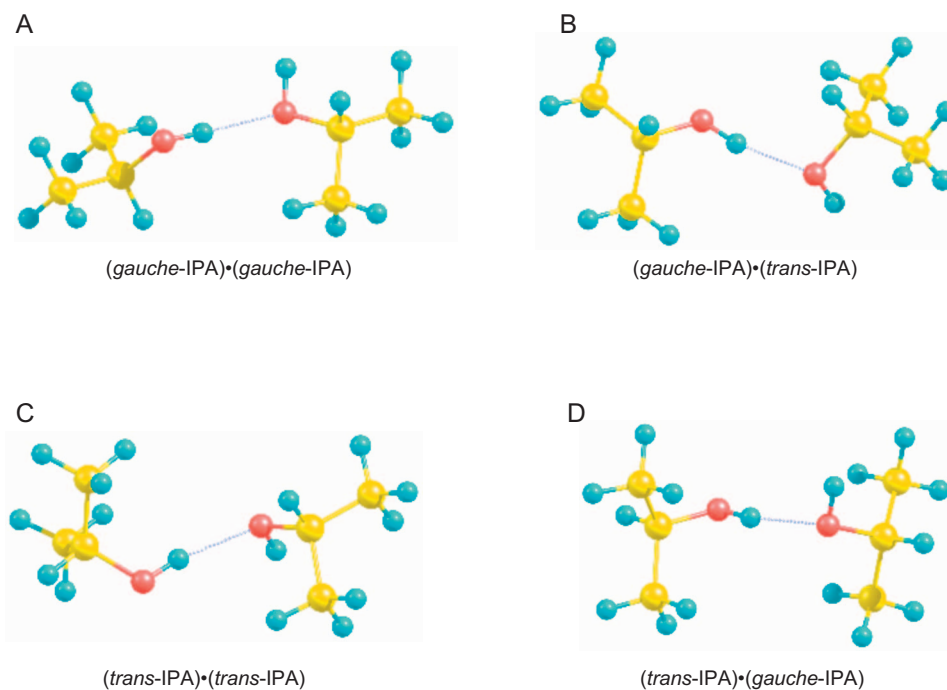


FIG. 7. (Color) B3LYP/6-31+G(d) structures of chainlike IPA dimer isomers: (a) *gauche*-IPA·*gauche*-IPA, (b) *gauche*-IPA·*trans*-IPA, (c) *trans*-IPA·*trans*-IPA, and (d) *trans*-IPA·*gauche*-IPA. X·Y means X is hydrogen bonded to Y.

the experimental value of  $27\text{ cm}^{-1}$ . Therefore, while calculations slightly overestimate the redshift from the hydrogen bonding interactions ( $3462$  and  $3483\text{ cm}^{-1}$  versus  $3517$  and  $3544\text{ cm}^{-1}$ ), the trends predicted for *gauche*-IPA·*gauche*-IPA and *trans*-IPA·*gauche*-IPA are consistent with the experimental data. Thus, of the four possible chainlike cluster isomers depicted in Fig. 7, the *gauche*-IPA·*gauche*-IPA and *trans*-IPA·*gauche*-IPA isomers [Figs. 7(a) and 7(d)] are generated with the highest concentration under the current conditions. The *gauche* conformer is accepting a hydrogen bond in both cases. This type of a single hydrogen bond donor–hydrogen bond acceptor structure has also been observed in water,<sup>1-6</sup> methanol,<sup>15,22</sup> and ethanol<sup>33</sup> dimer clusters. While dimer isomers with the *gauche* conformer as the hydrogen bond acceptor are identified by the IR spectrum, those with the *trans* conformer as the hydrogen bond acceptor are not observed. Assuming that a free OH group that accepts a hydrogen bond will undergo an approximately  $11\text{ cm}^{-1}$  redshift in its OH stretch energy, as observed for the *gauche*-IPA·*gauche*-IPA and *trans*-IPA·*gauche*-IPA isomers, the absence of a transition near  $3626\text{ cm}^{-1}$  indicates that dimer isomers with a *trans* hydrogen bond acceptor [the *gauche*-IPA·*trans*-IPA and *trans*-IPA·*trans*-IPA isomers] are not generated in the expansion. According to DFT calculations (Table II), the observed *gauche*-IPA·*gauche*-IPA and *trans*-IPA·*gauche*-IPA isomers are the most and the least stable, respectively, while *gauche*-IPA·*trans*-IPA and *trans*-IPA·*trans*-IPA are more stable than the *trans*-IPA·*gauche*-IPA isomer. One possible reason for the absence of the *gauche*-IPA·*trans*-IPA isomer is that its formation pathway is not kinetically or dynamically favorable during the cooling process in the expansion. Genera-

TABLE II. B3LYP/6-31+G(d) relative energies of neutral 2-propanol (IPA) clusters. Energy values ( $\Delta E_{\text{BSSE}}$ ) are corrected for basis set superposition error (BSSE) by counterpoise calculations.  $g = \textit{gauche}$  and  $t = \textit{trans}$ . X·Y means X is hydrogen bonded to Y.

$((\text{CH}_3)_2\text{CHOH})_n$	Isomers	$\Delta E_{\text{BSSE}}$ (eV)
2 chainlike	$(g\text{-IPA}) \cdot (g\text{-IPA})$	0.0000
	$(g\text{-IPA}) \cdot (t\text{-IPA})$	0.0012
	$(t\text{-IPA}) \cdot (t\text{-IPA})$	0.0188
	$(t\text{-IPA}) \cdot (g\text{-IPA})$	0.0227
3 cyclic	$(g\text{-IPA}) \cdot (g\text{-IPA}) \cdot (g\text{-IPA})$	0.0000
	$(g\text{-IPA}) \cdot (g\text{-IPA}) \cdot (t\text{-IPA})$	0.0169
	$(g\text{-IPA}) \cdot (t\text{-IPA}) \cdot (t\text{-IPA})$	0.0395
	$(t\text{-IPA}) \cdot (t\text{-IPA}) \cdot (t\text{-IPA})$	0.0547
4 cyclic	$(g\text{-IPA}) \cdot (g\text{-IPA}) \cdot (g\text{-IPA}) \cdot (g\text{-IPA})$	0.0000
	$(g\text{-IPA}) \cdot (g\text{-IPA}) \cdot (g\text{-IPA}) \cdot (t\text{-IPA})$	0.0162
	$(g\text{-IPA}) \cdot (t\text{-IPA}) \cdot (g\text{-IPA}) \cdot (t\text{-IPA})$	0.0301
	$(g\text{-IPA}) \cdot (g\text{-IPA}) \cdot (t\text{-IPA}) \cdot (t\text{-IPA})$	0.0358
	$(g\text{-IPA}) \cdot (t\text{-IPA}) \cdot (t\text{-IPA}) \cdot (t\text{-IPA})$	0.0419
	$(t\text{-IPA}) \cdot (t\text{-IPA}) \cdot (t\text{-IPA}) \cdot (t\text{-IPA})$	0.0479
4 3+1	$[(g\text{-IPA}) \cdot (g\text{-IPA}) \cdot (g\text{-IPA})] \cdot (g\text{-IPA})$	0.2605
	$[(g\text{-IPA}) \cdot (t\text{-IPA}) \cdot (t\text{-IPA})] \cdot (g\text{-IPA})$	0.2885
	$[(g\text{-IPA}) \cdot (g\text{-IPA}) \cdot (g\text{-IPA})] \cdot (t\text{-IPA})$	0.2915
	$[(g\text{-IPA}) \cdot (t\text{-IPA}) \cdot (g\text{-IPA})] \cdot (g\text{-IPA})$	0.2938
	$[(t\text{-IPA}) \cdot (t\text{-IPA}) \cdot (t\text{-IPA})] \cdot (g\text{-IPA})$	0.3111
	$[(g\text{-IPA}) \cdot (t\text{-IPA}) \cdot (t\text{-IPA})] \cdot (t\text{-IPA})$	0.3114
	$[(g\text{-IPA}) \cdot (g\text{-IPA}) \cdot (t\text{-IPA})] \cdot (t\text{-IPA})$	0.3170
	$[(t\text{-IPA}) \cdot (t\text{-IPA}) \cdot (t\text{-IPA})] \cdot (t\text{-IPA})$	0.3348

tion of the  $(\textit{trans}\text{-IPA}) \cdot (\textit{trans}\text{-IPA})$  isomer may also be hindered for a similar reason, but another possibility is the very low concentration of the *trans* monomers in the beam, as it is not identified in the IPA monomer IR spectra. The broad enhancement centered near  $3414 \text{ cm}^{-1}$  in the dimer IR spectrum [Fig. 6(a)] originates mostly from the trimer and possibly from the tetramer. The successive loss of monomers from the tetramer would arise through multiphoton absorption near  $3350 \text{ cm}^{-1}$ .

As mentioned above, the trimer has two VUV induced fragmentation pathways, which result in the  $m/z=121$  and  $165$  amu ions (Fig. 2). A broad, redshifted dip, approximately  $200 \text{ cm}^{-1}$  from the IPA monomer free OH stretch, dominates each trimer IR spectrum [Figs. 6(b) and 6(c)]. Thus the trimer has a cyclic structure with all OH groups involved in hydrogen bonding. This is also evidenced by the apparent absence of a free OH stretch feature in each spectrum. The trimer IR spectra show that the hydrogen bonded OH stretches of this species, which are observed in the two VUV ionization channels, occur at different IR photon energies ( $3482 \text{ cm}^{-1}$  in the  $m/z=121$  amu mass channel and  $3431 \text{ cm}^{-1}$  in the  $m/z=165$  amu mass channel). If the trimer cluster consists of only one isomer type, the OH stretch features should appear at similar IR photon energies regardless of the fragmentation channel. This OH stretch energy difference indicates that different trimer isomers exist in the beam. Since a cyclic geometry is the only possible trimer structure with all OH groups participating in hydrogen

bonding (i.e., hydrogen bond accepting and donating simultaneously), the isomer difference must arise from different combinations of *gauche* and *trans* monomer conformations. Figure 8 shows four possible cyclic trimer isomers:  $(\textit{gauche}\text{-IPA}) \cdot (\textit{gauche}\text{-IPA}) \cdot (\textit{gauche}\text{-IPA})$ ,  $(\textit{gauche}\text{-IPA}) \cdot (\textit{gauche}\text{-IPA}) \cdot (\textit{trans}\text{-IPA})$ ,  $(\textit{gauche}\text{-IPA}) \cdot (\textit{trans}\text{-IPA}) \cdot (\textit{trans}\text{-IPA})$ , and  $(\textit{trans}\text{-IPA}) \cdot (\textit{trans}\text{-IPA}) \cdot (\textit{trans}\text{-IPA})$ . While an unambiguous, specific isomer assignment is not possible based on the current data alone due to the intrinsically broad hydrogen bonded OH stretch transitions, one can infer from the IR spectra that trimer isomers that fragment into the  $m/z=121$  amu mass channel contain a greater number of *gauche* conformers than those that fragment into the  $m/z=165$  amu mass channel. As for the case of the dimer, this assignment is also based on the fact that the hydrogen bonded OH stretch of a *gauche* monomer occurs at higher energy than that of a *trans* monomer.

DFT calculations (Table II) predict that isomers with more *gauche* conformers are more stable, with the cyclic  $(\textit{gauche}\text{-IPA}) \cdot (\textit{gauche}\text{-IPA}) \cdot (\textit{gauche}\text{-IPA})$  being the most stable isomer. The significance of this result is that the VUV induced cluster fragmentation pathway is isomer dependent. This is a cluster analog of isomer specific fragmentation behavior of neutral molecules observed in our previous study<sup>54</sup> of aliphatic amino acids. Moreover, enhancements observed in the two trimer IR spectra [Figs. 6(b) and 6(c)] also occur at different photon energies, centered near  $3326$  and  $3253 \text{ cm}^{-1}$  for the  $m/z=121$  and  $165$  amu mass channels, respectively. Both of these features partially overlap with the pentamer IR spectrum [Fig. 6(e)]. Thus, larger clusters ( $n \geq 5$ ) may absorb more than one IR photon to undergo successive IPA monomer losses and eventually fragment into trimer related mass channels. Fragmentation pathways can thus be conformer selective, such that one cluster isomer group fragments to trimer isomers dominated by *gauche* conformers, while another group fragments to trimer isomers dominated by *trans* conformers.

IR spectra of the tetramer and pentamer [Figs. 6(d) and 6(e)] show a broad transition in a typical region for hydrogen bonded OH stretches. The spectra in this region are highly reminiscent of a liquid IPA IR spectrum,<sup>35</sup> and no free OH stretches are observed for these clusters. The absence of free OH stretches and the broadness of the hydrogen bonded OH transitions indicate that larger sized clusters are dominated by hydrogen bonding networks and the presence of several isomers.

Based on our DFT calculations and previous reports on other alcohol clusters,<sup>18,32</sup> two general types of IPA tetramer isomers can be identified: A cyclic form in which each of the four IPA molecules accepts and donates a hydrogen bond; and a 3+1 form in which an IPA molecule is hydrogen bonded to one of the molecules in a cyclic trimer. According to this scheme, at least 30 possible tetramer isomer geometries can be identified due to various possible combinations of the *gauche/trans* conformers and the three possible hydrogen bond accepting sites in the trimer structure. The relative energy value of the most stable structure in each isomer type is listed in Table II. Six of the structures are cyclic and eight are of the 3+1 form. Although both types of structures are

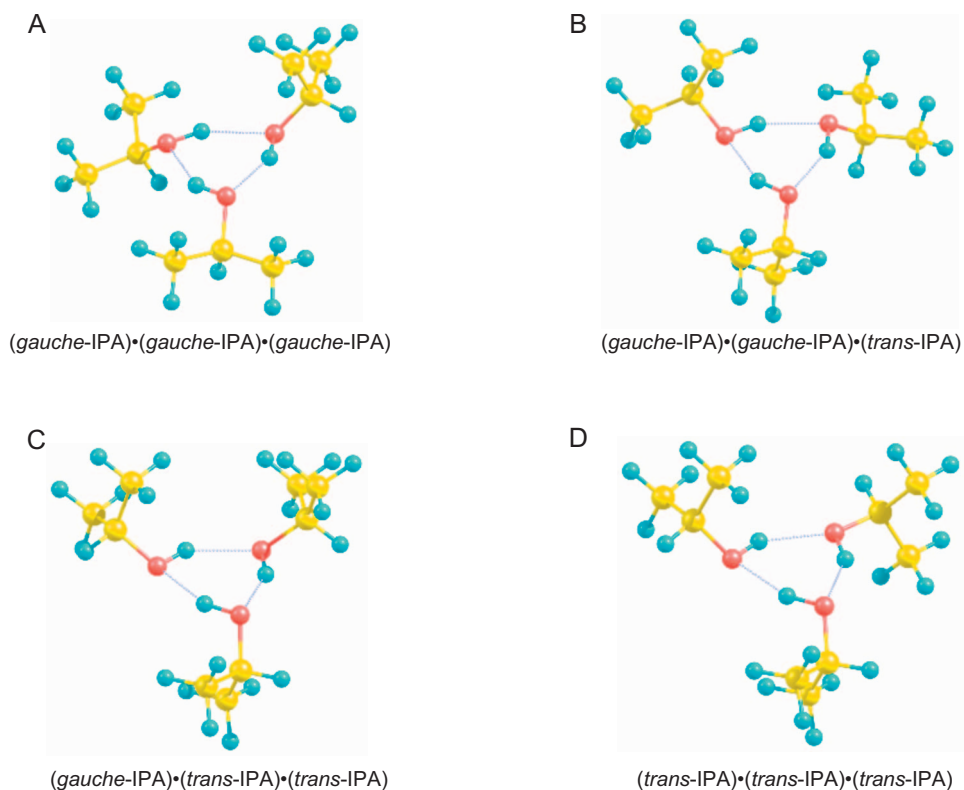


FIG. 8. (Color) B3LYP/6-31+G(d) structures of cyclic IPA trimer isomers: (a) (*gauche*-IPA)·(*gauche*-IPA)·(*gauche*-IPA), (b) (*gauche*-IPA)·(*gauche*-IPA)·(*trans*-IPA), (c) (*gauche*-IPA)·(*trans*-IPA)·(*trans*-IPA), and (d) (*trans*-IPA)·(*trans*-IPA)·(*trans*-IPA).

qualitatively consistent with the IR spectrum because neither has a free OH band and hydrogen bonds dominate the structures, the spectrum is most likely from cyclic tetramer isomers only. The reason to suggest this is that in the 3+1 structures, the IPA molecule hydrogen bonded to one of the molecules in the cyclic trimer is in a single hydrogen bond donating configuration, which should result in an extra feature that is only slightly redshifted from the free OH stretch, as observed for the dimer. Since the broad tetramer transition in Fig. 6(d) is redshifted by nearly  $330\text{ cm}^{-1}$  from the IPA monomer OH stretch, this feature is most probably from cyclic tetramer isomers only. Also, cyclic structures are on average  $0.272\text{ eV}$  more stable than 3+1 structures (Table II), and cyclic structures with a greater number of the *gauche* conformers are more stable than those with more *trans* conformers. A theoretical investigation<sup>31</sup> of other alcohol systems also predicts cyclic forms to be more stable due to enhanced hydrogen bond cooperativity. The tetramer spectrum shows a small enhancement near  $3200\text{ cm}^{-1}$ , suggesting that larger clusters ( $n \geq 6$ ) in the molecular beam can fragment into the tetramer mass channel.

We have not carried out theoretical structural analysis for pentamer isomers, but based on previous gas phase studies<sup>15,18,22,30–33</sup> of other alcohol clusters, they will also most likely have five membered cyclic structures. The loss of one or more IPA molecules from the clusters is reflected in the monomer IR spectrum in the  $3200\text{--}3440\text{ cm}^{-1}$  range as a broad unresolved transition.

Partially resolved CH stretches of IPA clusters are observed near  $2975\text{ cm}^{-1}$ . Their peak positions do not change significantly with increasing cluster size; thus the CH and

$\text{CH}_3$  groups are not involved in hydrogen bonding interactions. With the exception of trimer isomers that yield the  $m/z=121$  amu ion, all clusters display an ion dip near this photon energy. The dimer isomers ( $m/z=105$  amu) and the trimer isomers that yield the  $m/z=165$  amu ion fragment into the monomer mass channel at  $2975\text{ cm}^{-1}$  IR photon energy. Larger clusters (tetramer and pentamer) can also contribute to the peak intensity enhancements near  $2975\text{ cm}^{-1}$  in both the monomer parent ( $m/z=60$  amu) and trimer ( $m/z=121$  amu) mass channels after VUV ionization.

## B. VUV/IR photodissociation spectroscopy of ionic IPA monomer and clusters

Figures 9(a)–9(c) show the IR spectra of the IPA monomer cation detected in  $m/z=44$ ,  $45$ , and  $60$  amu mass channels in the  $2800\text{--}3800\text{ cm}^{-1}$  region. Calculated IPA cation isomer structures and their scaled harmonic vibrational energies are shown in Figs. 9(d) and 9(e). The experimental and theoretical vibrational energy values are listed in Table III. The IR spectrum in the  $m/z=44$  amu mass channel shows no features associated with OH stretches, while a gradual increase in the ion intensity is observed toward the CH stretch region. On the other hand, the sharp doublet centered at  $3483$  and  $3516\text{ cm}^{-1}$  as well as a broad enhancement in the CH stretch region in IR spectrum in the  $m/z=45$  amu mass channel appear as dips in the  $m/z=60$  amu mass channel. The doublet corresponds to free OH stretches of the parent IPA cation. The similarity between these two IR spectra obtained in the two different mass channels indicates that when the parent ion ( $m/z=60$  amu) absorbs IR photons in

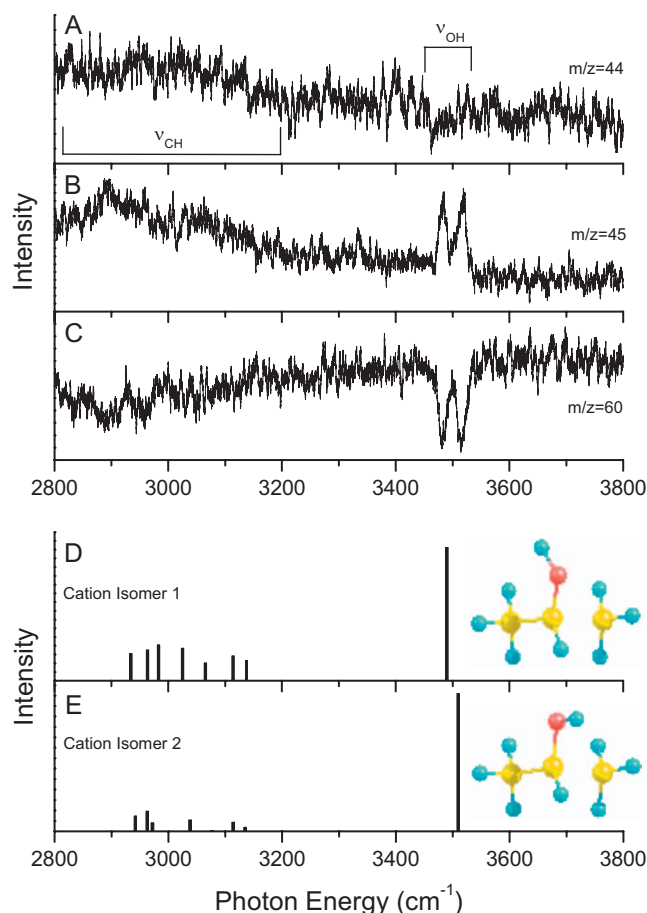


FIG. 9. (Color) IR spectra of the IPA parent cations obtained by monitoring ion intensity changes of (a)  $m/z=44$  amu, (b)  $m/z=45$  amu, and (c)  $m/z=60$  amu ion mass channels. Free OH stretch features of the parent cation centered at 3483 and 3516  $\text{cm}^{-1}$  are reflected in the  $m/z=45$  amu ion channel, and the broad CH stretch feature (2800–3200  $\text{cm}^{-1}$ ) appears in both fragment ion channels. MP2/aug-cc-pVDZ structures and harmonic vibrational energies of (d) isomer type I and (e) isomer type II IPA parent cations. The energies are scaled by 0.9593.

TABLE III. Experimentally obtained free OH stretch ( $\nu_{\text{OH}}$ ) energies of IPA monomer and clusters. Harmonic OH stretch energy values of two adiabatic IPA cations are shown for comparison. Calculations are carried out at the MP2/aug-cc-pVDZ level and the vibrational energies are scaled by the factor of 0.9593.

Experiment		
Ion	Ion $m/z$	$\nu_{\text{OH}}$ ( $\text{cm}^{-1}$ )
$\text{CH}_3\text{COH}^+$	44	...
$\text{CH}_3\text{CHOH}^+$	45	3485, 3519
$(\text{CH}_3)_2\text{CHOH}^+$	60	3481, 3515
$(\text{CH}_3)_2\text{CHOH} \cdot \text{CH}_3\text{CHOH}^+$	105	3639
$((\text{CH}_3)_2\text{CHOH})_2 \cdot \text{H}^+$	121	3634
$((\text{CH}_3)_2\text{CHOH})_2 \cdot \text{CH}_3\text{CHOH}^+$	165	3636
$((\text{CH}_3)_2\text{CHOH})_3 \cdot \text{H}^+$	181	3628
$((\text{CH}_3)_2\text{CHOH})_4 \cdot \text{H}^+$	241	3630
Calculation		
Isomer 1	60	3490
Isomer 2	60	3510

the CH and OH stretch regions, the *intramolecular* vibrational redistribution (as opposed to *intermolecular* vibrational redistribution in clusters) process facilitates the  $\text{C}_\alpha\text{-C}_\beta$  bond dissociation of the IPA cation and leads to enhancement of the loss of  $\text{CH}_3$  (increase in the  $m/z=45$  amu mass channel); some of the IVR energy from CH stretches partially enhances the loss of  $\text{CH}_4$ , as well.

One curiosity in the IR spectra of the IPA cation is the presence of two OH stretch features (the doublet centered at 3483 and 3516  $\text{cm}^{-1}$ ). Since only the *gauche* conformation of the neutral monomer is produced in the current study, both features must be the OH stretches of the parent cation generated by VUV ionization of the *gauche*-IPA. The TOF mass spectrum unambiguously shows that the losses of  $\text{CH}_3$  and  $\text{CH}_4$  are the primary VUV induced fragmentation pathways of *gauche*-IPA, but it does not provide information on ion structures and behavior. *Ab initio* calculations show that two isomeric forms of the IPA parent cation [Figs. 9(d) and 9(e) insets] can be generated. The difference between the two is orientation of the hydrogen of the OH group, and isomer I is more stable than isomer II by 0.0060 eV (isomer II is also shown in Fig. 3 as the ion that undergoes the barrierless loss of  $\text{CH}_3$ ). Their scaled harmonic frequencies are also in excellent agreement with the IR spectra. Hence, some of the Franck–Condon *gauche*-IPA parent cations undergo OH group reorientation as they evolve to the adiabatic state; the similar OH stretch peak intensities indicate that the population ratio of the two cation isomer types is about 1. VUV/IR spectroscopy thus reveals an additional reaction pathway through which the parent IPA cation fragments. The three ion fragmentation pathways of the *gauche*-IPA cation are (1) barrierless loss of  $\text{CH}_3$ , (2) hydrogen transfer from  $\text{C}_\alpha\text{H}$  to  $\text{CH}_3$  and loss of  $\text{CH}_4$ , and (3) reorientation of the OH group and loss of  $\text{CH}_3$ .

IR spectra of cation clusters are presented in Fig. 10. CH and hydrogen bonded OH stretches are observed as weak, broad transitions in the 2800–3500  $\text{cm}^{-1}$  region, and free OH stretch features appear near 3635  $\text{cm}^{-1}$ . The CH and hydrogen bonded OH stretches are more apparent for the  $((\text{CH}_3)_2\text{CHOH})_3 \cdot \text{H}^+$  and  $((\text{CH}_3)_2\text{CHOH})_4 \cdot \text{H}^+$  ions, implying that larger protonated clusters mostly fragment into these two channels upon IR photon absorption. The IR signals of cation clusters are weak for two possible reasons: Weak ion mass spectral intensities; and stronger hydrogen bonds as a result of the presence of an extra positive charge. The latter partially reduces fragmentation, in general. As mentioned earlier, two types of cations,  $((\text{CH}_3)_2\text{CHOH})_{n-1} \cdot \text{CH}_3\text{CHOH}^+$  ( $n=2$  and 3) and  $((\text{CH}_3)_2\text{CHOH})_{n-1} \cdot \text{H}^+$  ( $n=3-5$ ), are generated by VUV ionization of IPA clusters. Cluster fragmentation can only occur through the loss of individual IPA molecules from the same type of ion clusters because chemical bonds cannot be broken by the IR energy in the range employed in this study [i.e.,  $((\text{CH}_3)_2\text{CHOH})_{n-2} \cdot \text{CH}_3\text{CHOH}^+$  cannot be generated from  $((\text{CH}_3)_2\text{CHOH})_{n-1} \cdot \text{H}^+$ ]. Therefore, the enhancement of the  $((\text{CH}_3)_2\text{CHOH}) \cdot \text{CH}_3\text{CHOH}^+$  ion ( $m/z=105$  amu) near 3635  $\text{cm}^{-1}$  is a result of the loss of one IPA molecule from the  $((\text{CH}_3)_2\text{CHOH})_2 \cdot \text{CH}_3\text{CHOH}^+$  ion ( $m/z=165$  amu) near this IR photon energy. Similarly, the OH stretch feature of the  $((\text{CH}_3)_2\text{CHOH})_2 \cdot \text{H}^+$  ion ( $m/z$

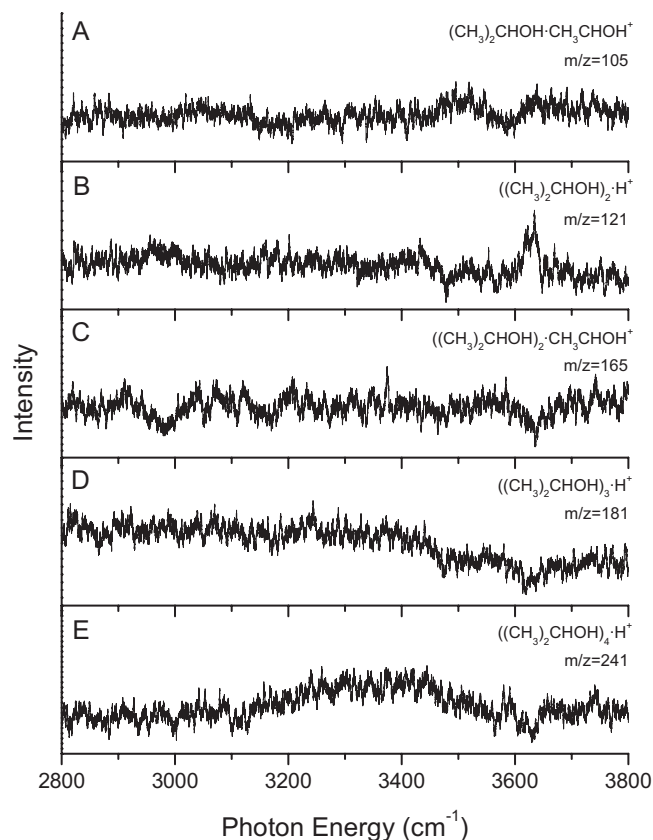


FIG. 10. IR spectra of the IPA cation clusters: ionic molecular complex clusters  $((\text{CH}_3)_2\text{CHOH})_x \cdot \text{CH}_3\text{CHOH}^+$  and protonated clusters  $((\text{CH}_3)_2\text{CHOH})_y \cdot \text{H}^+$ : (a)  $x=1$ , (b)  $y=2$ , (c)  $x=2$ , (d)  $y=3$ , and (e)  $y=4$ . The free OH stretch mode centered near  $3635 \text{ cm}^{-1}$  is observed for each cluster.

$=121 \text{ amu}$ ) is from fragmentations of  $((\text{CH}_3)_2\text{CHOH})_3 \cdot \text{H}^+$  and  $((\text{CH}_3)_2\text{CHOH})_4 \cdot \text{H}^+$  ( $m/z=181$  and  $241 \text{ amu}$ ) and also possibly from larger protonated clusters. This transition is relatively more intense since at least two clusters are fragmenting into the  $m/z=121 \text{ amu}$  channel. The free OH stretch feature near  $3635 \text{ cm}^{-1}$  in each spectrum indicates that at least one IPA molecule which only accepts a hydrogen bond (but does not donate one) exists in each cluster and that this molecule remains in a similar environment with the increasing cluster size. In the small cluster cation size range studied, the presence of free OH stretches implies that those cation clusters have relatively open structures.

## V. CONCLUSIONS

We have carried out IR/VUV nonresonant photoionization spectroscopy of the neutral IPA monomer and its clusters and VUV/IR photodissociation spectroscopy of the ionic IPA monomer, ionic molecular complex clusters, and protonated clusters.

The IR/VUV study shows that *gauche*-IPA is the only monomer conformer generated in the supersonic expansion. It undergoes loss of  $\text{CH}_3$  and hydrogen transfer mediated loss of  $\text{CH}_4$  following VUV ionization and internal rearrangement. The fragmentation pathways of the IPA related clusters are size dependent: An ionic molecular complex cluster  $((\text{CH}_3)_2\text{CHOH})_{n-1} \cdot \text{CH}_3\text{CHOH}^+$  is generated from the dimer; protonated clusters  $((\text{CH}_3)_2\text{CHOH})_{n-1} \cdot \text{H}^+$  are generated

from the tetramer and pentamer; and both types of ionic clusters are produced from VUV ionization of the trimer. Analysis of the dimer IR spectrum and calculations suggest that two neutral dimer isomers are generated in the expansion, with the *gauche* IPA conformer accepting a hydrogen bond from the other molecule of the dimer and forming a chainlike structure in each isomer. The trimer IR spectra and calculations show that several isomers are present in the supersonic expansion. Trimer isomers have cyclic structures without any free OH groups, and isomers with more *gauche* conformers generate the protonated cluster  $((\text{CH}_3)_2\text{CHOH})_2 \cdot \text{H}^+$  ( $m/z=121 \text{ amu}$ ), while those with more *trans* conformers generate the ionic molecule cluster  $((\text{CH}_3)_2\text{CHOH})_2 \cdot \text{CH}_3\text{CHOH}^+$  ( $m/z=165 \text{ amu}$ ) following VUV ionization. The large redshift of OH stretches observed in the IR spectra of the tetramer and pentamer is also consistent with cyclic structures of these clusters. DFT calculations show that, similar to the trimer structures, tetramer isomers consisting of a greater number of the *gauche* monomer are more stable. Larger clusters are also generated, and the IR spectrum of the tetramer shows that they can fragment into the tetramer related mass channel.

The VUV/IR spectra show that two IPA parent cation isomers are generated following neutral *gauche*-IPA ionization and show an additional VUV induced fragmentation pathway for the Franck–Condon IPA monomer cation: The OH group rotates to the opposite direction, further enabling  $\text{C}_\alpha\text{--C}_\beta$  dissociation that leads to loss of  $\text{CH}_3$ . Cation clusters fragment via the loss of one or more IPA molecules after absorbing IR photons. The relatively small sized ionic clusters studied in the present work apparently have open, not cyclic, structures.

## ACKNOWLEDGMENTS

The authors gratefully acknowledge support from USARO and NSF.

- M. F. Vernon, D. J. Krajnowich, H. S. Kwok, J. M. Lisy, Y.-R. Shen, and Y. T. Lee, *J. Chem. Phys.* **77**, 47 (1982).
- R. H. Page, J. G. Frey, Y.-R. Shen, and Y. T. Lee, *Chem. Phys. Lett.* **106**, 373 (1984).
- D. F. Coker, R. E. Miller, and R. O. Watts, *J. Chem. Phys.* **82**, 3554 (1985).
- Z. S. Huang and R. E. Miller, *J. Chem. Phys.* **88**, 8008 (1988).
- K. L. Busarow, R. C. Cohen, G. A. Blake, K. B. Laughlin, Y. T. Lee, and R. J. Saykally, *J. Chem. Phys.* **90**, 3937 (1989).
- Z. S. Huang and R. E. Miller, *J. Chem. Phys.* **91**, 6613 (1989).
- R. N. Pribble and T. S. Zwier, *Science* **265**, 75 (1994).
- J. D. Cruzan, M. G. Brown, K. Liu, L. B. Braly, and R. J. Saykally, *J. Chem. Phys.* **105**, 6634 (1996).
- C. J. Gruenloh, J. R. Carney, C. A. Arrington, T. S. Zwier, S. Y. Fredericks, and K. D. Jordan, *Science* **276**, 1678 (1997).
- J. Brudermann, U. Buck, and V. Buch, *J. Phys. Chem. A* **106**, 453 (2002).
- S. Hirabayashi and K. M. T. Yamada, *J. Chem. Phys.* **122**, 244501 (2005).
- F. Dong, S. Heinbuch, J. J. Rocca, and E. R. Bernstein, *J. Chem. Phys.* **124**, 224319 (2006).
- S. Hirabayashi and K. M. T. Yamada, *J. Mol. Struct.* **795**, 78 (2006).
- F. Huisken and M. Stemmler, *Chem. Phys. Lett.* **144**, 391 (1988).
- U. Buck, X. J. Gu, Ch. Lauenstein, and A. Rudolph, *J. Chem. Phys.* **92**, 6017 (1990).
- F. Huisken, A. Kulcke, C. Laush, and J. M. Lisy, *J. Chem. Phys.* **95**, 3924 (1991).

- <sup>17</sup> F. Huisken, M. Kaloudis, M. Koch, and O. Werhahn, *J. Chem. Phys.* **105**, 8965 (1996).
- <sup>18</sup> F. C. Hagemester, C. J. Gruenloh, and T. S. Zwier, *J. Phys. Chem. A* **102**, 82 (1998).
- <sup>19</sup> R. A. Provencal, J. B. Paul, K. Roth, C. Chapo, R. N. Casaes, R. J. Saykally, G. S. Tschumper, and H. F. Schaefer III, *J. Chem. Phys.* **110**, 4258 (1999).
- <sup>20</sup> Y. J. Shi, S. Consta, A. K. Das, B. Mallik, D. Lacey, and R. H. Lipson, *J. Chem. Phys.* **116**, 6990 (2002).
- <sup>21</sup> H. B. Fu, Y. J. Hu, and E. R. Bernstein, *J. Chem. Phys.* **124**, 024302 (2006).
- <sup>22</sup> Y. J. Hu, H. B. Fu, and E. R. Bernstein, *J. Chem. Phys.* **125**, 154306 (2006).
- <sup>23</sup> O. Kostko, L. Belau, K. R. Wilson, and M. Ahmed, *J. Phys. Chem. A* **112**, 9555 (2008).
- <sup>24</sup> E. Honegger and S. Leutwyler, *J. Chem. Phys.* **88**, 2582 (1988).
- <sup>25</sup> S. S. Xantheas and T. H. Dunning, Jr., *J. Chem. Phys.* **99**, 8774 (1993).
- <sup>26</sup> J. K. Kazimirski and V. Buch, *J. Phys. Chem. A* **107**, 9762 (2003).
- <sup>27</sup> G. S. Fanourgakis, E. Aprá, W. A. de Jong, and S. S. Xantheas, *J. Chem. Phys.* **122**, 134304 (2005).
- <sup>28</sup> A. Lenz and L. Ojamäe, *Chem. Phys. Lett.* **418**, 361 (2006).
- <sup>29</sup> S. Karthikeyan, N. J. Singh, and K. S. Kim, *J. Phys. Chem. A* **112**, 6527 (2008).
- <sup>30</sup> U. Buck, J.-G. Siebers, and R. J. Wheatly, *J. Chem. Phys.* **108**, 20 (1998).
- <sup>31</sup> A. K. Sum and S. I. Sandler, *J. Phys. Chem. A* **104**, 1121 (2000).
- <sup>32</sup> S. L. Boyd and R. J. Boyd, *J. Chem. Theory Comput.* **3**, 54 (2007).
- <sup>33</sup> Y. J. Hu, H. B. Fu, and E. R. Bernstein, *J. Chem. Phys.* **125**, 154305 (2006).
- <sup>34</sup> R. A. Provencal, R. N. Casaes, K. Roth, J. B. Paul, C. N. Chapo, R. J. Saykally, G. S. Tschumper, and H. F. Schaefer III, *J. Phys. Chem.* **104**, 1423 (2000).
- <sup>35</sup> H. Schaal, T. Häber, and M. A. Suhm, *J. Phys. Chem. A* **104**, 265 (2000).
- <sup>36</sup> D. Zimmermann, Th. Häber, H. Schaal, and M. A. Suhm, *Mol. Phys.* **99**, 413 (2001).
- <sup>37</sup> J.-C. Jiang, Y.-S. Wang, H.-C. Chang, S. H. Lin, Y. T. Lee, G. Niedner-Schatteburg, and H.-C. Chang, *J. Am. Chem. Soc.* **122**, 1398 (2000).
- <sup>38</sup> J.-W. Shin, N. I. Hammer, E. G. Diken, M. A. Johnson, R. S. Walters, T. D. Jaeger, M. A. Duncan, R. A. Christie, and K. D. Jordan, *Science* **304**, 1137 (2004).
- <sup>39</sup> M. Miyazaki, A. Fujii, T. Ebata, and N. Mikami, *Science* **304**, 1134 (2004).
- <sup>40</sup> J. M. Headrick, E. G. Diken, R. S. Walters, N. I. Hammer, R. A. Christie, J. Cui, E. M. Myshakin, M. A. Duncan, M. A. Johnson, and K. D. Jordan, *Science* **308**, 1765 (2005).
- <sup>41</sup> H.-C. Chang, J.-C. Jiang, S. H. Lin, Y. T. Lee, and H.-C. Chang, *J. Phys. Chem. A* **103**, 2941 (1999).
- <sup>42</sup> A. Fujii, S. Enomoto, M. Miyazaki, and N. Mikami, *J. Phys. Chem. A* **109**, 138 (2005).
- <sup>43</sup> S.-T. Tsai, J.-C. Jiang, M.-F. Lin, Y. T. Lee, and C.-K. Ni, *J. Chem. Phys.* **120**, 8979 (2004).
- <sup>44</sup> M. Eigen, *Angew. Chem., Int. Ed. Engl.* **3**, 1 (1964).
- <sup>45</sup> G. Zundel, in *The Hydrogen Bond—Recent Developments in Theory and Experiments. II. Structure and Spectroscopy*, edited by P. Schuster, G. Zundel, and C. Sandorfy (North-Holland, Amsterdam, 1976), pp. 683–766.
- <sup>46</sup> F. M. Benoit and A. G. Harrison, *J. Am. Chem. Soc.* **99**, 3980 (1977).
- <sup>47</sup> M. J. Frisch, G. W. Trucks, H. B. Schlegel *et al.*, GAUSSIAN 03, Revision C.02, Gaussian, Inc., Wallingford CT (2004).
- <sup>48</sup> C. Catlett *et al.*, in *TeraGrid: Analysis of Organization, System Architecture, and Middleware Enabling New Types of Applications, HPC and Grids in Action*, Advances in Parallel Computing Series, edited by L. Grandinetti (IOS, Amsterdam, 2007).
- <sup>49</sup> J.-W. Shin and E. R. Bernstein (unpublished).
- <sup>50</sup> H. L. Fang and D. A. C. Compton, *J. Phys. Chem.* **92**, 6518 (1988).
- <sup>51</sup> G. S. Fanourgakis, Y. J. Shi, S. Consta, and R. H. Lipson, *J. Chem. Phys.* **119**, 6597 (2003).
- <sup>52</sup> Y. J. Hu, H. B. Fu, and E. R. Bernstein, *J. Chem. Phys.* **125**, 184308 (2006).
- <sup>53</sup> Y. J. Hu, H. B. Fu, and E. R. Bernstein, *J. Chem. Phys.* **125**, 184309 (2006).
- <sup>54</sup> Y. Hu and E. R. Bernstein, *J. Chem. Phys.* **128**, 164311 (2008).